

# Composition-induced structural transitions in mixed rare-gas clusters

F. Calvo

*Laboratoire de Physique Quantique, IRSAMC, Université Paul Sabatier,  
118 Route de Narbonne, F31062 Toulouse Cedex, France*

E. Yurtsever

*Koç University, Rumelifeneriyolu, Sariyer, Istanbul 34450, Turkey*

The low-energy structures of mixed Ar–Xe and Kr–Xe Lennard-Jones clusters are investigated using a newly developed parallel Monte Carlo minimization algorithm with specific exchange moves between particles or trajectories. Tests on the 13- and 19- atom clusters show a significant improvement over the conventional basin-hopping method, the average search length being reduced by more than one order of magnitude. The method is applied to the more difficult case of the 38-atom cluster, for which the homogeneous clusters have a truncated octahedral shape. It is found that mixtures of dissimilar elements (Ar–Xe) favor icosahedral geometries over octahedra due to the reduced strain penalty. Conversely, octahedra are even more stable in Kr–Xe mixtures than in Kr<sub>38</sub> or Xe<sub>38</sub>, and they show a core-surface phase separation behavior. Finally, we correlate the relative stability of cubic structures in these clusters to the glassforming character of the bulk mixtures.

## I. INTRODUCTION

Clusters of heterogeneous materials show a much richer behavior than their homogeneous counterparts. In many bulk compounds, doping can significantly affect some global property, and alloying is a common way to tailor a completely new kind of material. At the mesoscale level, size is another complicating factor, giving rise to further changes with respect to the macroscopic object. To a large extent, most expectations of nanotechnology have been put into the electronic and catalytic properties of small atomic clusters. Therefore, it should not be surprising that numerous theoretical studies of mixed clusters were devoted to bimetallic clusters. In particular, there has been a significant amount of work at the level of sophisticated electronic structure calculations,<sup>1,2,3</sup> but these were often limited to small sizes due to the numerical effort involved. On a different scale of chemical complexity, many studies have been carried out using explicit, empirical force fields<sup>4,5,6,7,8,9,10,11,12</sup> in order to investigate the segregation properties of these clusters.

Among the features that determine whether binary systems undergo mixing or phase separation, surface energies and interactions between unlike atoms are two competitive and important factors. Under appropriate conditions, the kinetics of formations can also be crucial.<sup>13</sup>

In comparison, finite-size compounds made of rare-gas atoms have received much less attention. Fortunately, they can be quite safely described using simple pairwise potentials such as Lennard-Jones (LJ). Hence they are much more convenient to study in a broad size range, not only for their structure but also their dynamics of thermodynamics. It is known from previous studies that the topography of the potential energy surfaces of homogeneous LJ clusters can be very peculiar, as for the sizes 38 or 75.<sup>14</sup> The multiple-funnel structure of these energy landscapes makes it especially hard to locate the

most stable structures (global minima) or to simulate the finite-temperature behavior of these clusters in an ergodic way. The effects of mixing different rare-gas atoms on cluster structure and thermodynamics have been studied for the specific size 13 by Frantz on the examples of Ar–Kr mixtures<sup>15</sup> as well as Ne–Ar mixtures.<sup>16</sup> Fanourgakis *et al.* have recently also investigated these latter compounds.<sup>17</sup> A systematic work of Ar–Xe mixed clusters of 13 and 19 atoms has been carried out by Munro and coworkers,<sup>18</sup> including some global optimization and Monte Carlo simulations.

The main conclusion of these studies is that atomic heterogeneity can be responsible for a drastic increase in complexity of the energy landscapes of rare-gas clusters. This complexity is manifested by numerous new low-lying minima in competitive funnels, characterized by the same overall geometrical arrangement but different permutations of unlike atoms. Following Jellinek and Krissinel,<sup>4</sup> we will refer to such isomers as “homotops.” The presence of several homotops on a given energy landscape often induces solid-solid transitions, which can be detected by some feature in the heat capacity.<sup>15,16,17,18,19</sup> As shown by Munro *et al.*,<sup>18</sup> the various funnels corresponding to different homotops of a same geometry are separated by significant energy barriers. This explains the difficulty or even failure of simulation methods to achieve ergodic sampling of these systems, albeit small.<sup>18</sup> A similar situation is found in Lennard-Jones polymers,<sup>20</sup> where a large number of isomers are based on the same geometrical arrangement, differing only in the path linking the monomers.

Beyond the actual rare-gases, binary Lennard-Jones compounds have been investigated in both the cluster and bulk regimes. Clarke and coworkers looked at phase separation of small particles with equal compositions.<sup>21</sup> Based on Monte Carlo simulations, they sketched a phase diagram in the general structure of liquid clusters. Bulk binary Lennard-Jones systems have been seen to provide relatively simple numerical models for glass

formation.<sup>22,23,24,25,26,27</sup> Most often, the LJ interactions in such studies have been tuned in a non-additive way in order to hinder crystallisation. In another related work, Lee and coworkers<sup>28</sup> have investigated the role of atomic size ratio in binary and ternary metallic alloys.

Interestingly, several links between the physics and chemistry of clusters and those of supercooled liquids and glasses have been established since the pioneering work by Frank.<sup>29</sup> The initial suggestion that the local order in simple liquids is not crystalline but icosahedral<sup>29</sup> (more generally polytetrahedral) has since been verified experimentally<sup>30</sup> and theoretically.<sup>22,31</sup> From the clusters viewpoint, the favored finite-size structures of good model glassformers have been shown by Doye and coworkers to be polytetrahedral.<sup>32</sup>

The 38-atom homogeneous Lennard-Jones cluster is known to show some glassy properties, especially slow relaxation to the ground state,<sup>33</sup> due to the competition between two stable funnels on the energy landscape, corresponding to truncated octahedral and icosahedral shapes, respectively. Due to entropic effects,<sup>33,34</sup> a solid-solid transition occurs between the two funnels, at temperatures lower than the melting point. The crystal-like configuration of this cluster makes it a good candidate to further investigate the relationship between cluster structure and criteria for glassification.

Because homogeneous LJ<sub>38</sub> constitutes a relatively difficult task for global optimization algorithms, binary clusters of the same size can be expected to be much worse. In this paper, we propose a simple but efficient way to deal with the multiple new minima introduced by unlike atoms within a general Monte Carlo global minimization scheme. This algorithm will then be applied to the 38-atom case, in mixtures of Xe with either Ar or Kr atoms. In the next section, we present the method and test it on the simple cases of the 13- and 19-atom clusters. In Sec. III we give our results obtained at size 38 and we correlate them to the different glassforming abilities of the bulk mixtures. We finally conclude in Sec. IV.

## II. METHODS

Global optimization of cluster structure<sup>35</sup> is currently best achieved using either genetic algorithms<sup>36</sup> or the Monte Carlo+minimization method,<sup>37</sup> also known as basin-hopping (BH).<sup>38</sup> The case of homogeneous Lennard-Jones clusters is among the most documented of cluster physics, and an up-to-date table of putative global minima can be found in Ref. 39. Even though it can never be guaranteed that global minimization has been successful, it is likely that all important structural forms of LJ clusters have been found up to more than 100 atoms. These include icosahedral, truncated octahedral, decahedral as well as tetrahedral arrangements.

Compared to homogeneous clusters, the available data on heterogeneous systems is rather scarce. Besides the specific works by Frantz on the 13-atom Ne-Ar and Kr-

Ar clusters,<sup>15,16</sup> Munro *et al.* used a parallel version of the BH scheme, similar to the replica-exchange Monte Carlo method,<sup>40</sup> where several trajectories are run simultaneously at various temperatures.<sup>18</sup> Although these authors looked at moderately large clusters, they reported significant difficulties to locate global minima at specific compositions, as in Xe<sub>10</sub>Ar<sub>3</sub> or Xe<sub>13</sub>Ar<sub>6</sub>, for instance.<sup>18</sup>

A natural problem occurring using the basin-hopping method is that many of the low-lying minima are expected to be related to each other via particle exchange. Such a process only occurs via large deformations of the remaining cluster, hence it is quite improbable. As in condensed matter physics,<sup>41,42,43</sup> allowing exchange moves between particles as a possible Monte Carlo step may result in notably faster convergence, provided that the interactions are not too dissimilar.

In the framework of global optimization methods, the local minimization stage removes the possible energetic penalty associated to replacing a small atom by a bigger one. We can thus expect some increased efficiency of the algorithm in case of multiple homotops. Other improvements are possible. Since the tetrahedral isomer of LJ<sub>98</sub> was discovered using a variant of the BH method,<sup>44</sup> it has been shown that temperature is not a key parameter of this algorithm, and that it can be set to zero without loss in efficiency. The extra numerical cost of running parallel trajectories at various temperatures can thus be converted into running them at various compositions. For a X<sub>p</sub>Y<sub>n-p</sub> compound, each of the  $n$  trajectories is then labelled with the number  $p$  of X atoms, running from 0 to  $p$ . Exchange moves between adjacent trajectories (from  $p$  to  $p+1$ ) thus need to incorporate the transmutation of two atoms (one for each configuration) into the other atom type to preserve composition. As in most Monte Carlo processes, the probability of attempting such moves must be set in advance as a parameter.

The global optimization algorithm can thus be summarized into its main steps. Keeping the above notations for atom types, and denoting  $\mathbf{R}_i^{(p)}$  the configuration at step  $i$  of trajectory  $p$ , we start the optimization process using fully random configurations, but locally optimized.

1. With probability  $P_{\text{ex}}$ , it is decided whether an exchange between adjacent trajectories will be attempted or not. If so, then the two trajectories involved in the exchange are determined randomly.
2. For each composition  $p$  not concerned by any exchange, a new configuration  $\mathbf{R}_{i+1}^{(p)}$  is generated from  $\mathbf{R}_i^{(p)}$  using either several particle exchanges or large atomic moves. The probability to select particle exchanges is denoted  $P_{\text{swap}}$ , and the number of simultaneous exchanges is allowed to fluctuate randomly between 1 and  $N_{\text{swap}}^{\text{max}}$ . If atomic moves are selected, then each atom is displaced randomly around its previous location in the three directions by a random amount of maximum magnitude  $h^{(p)}$ . In both cases,  $\mathbf{R}_{i+1}^{(p)}$  is obtained after local minimization.

3. In case of an exchange between adjacent trajectories, the two configurations  $\mathbf{R}_i^{(p)}$  and  $\mathbf{R}_i^{(p+1)}$  corresponding to these trajectories are then swapped, one X atom of  $\mathbf{R}_i^{(p)}$  being transmuted into Y, and one Y atom of  $\mathbf{R}_i^{(p+1)}$  being transmuted into X. Again, the configurations  $\mathbf{R}_{i+1}^{(p)}$  and  $\mathbf{R}_{i+1}^{(p+1)}$  are obtained after local minimization.
4. As a zero temperature process, each new configuration is kept only if its energy is lower than the energy at the previous step. Otherwise it is rejected and replaced by the previous configuration.

The algorithm has two main parameters, namely  $P_{\text{ex}}$  and  $P_{\text{swap}}$ . The maximum number of particle exchange moves,  $N_{\text{swap}}^{\text{max}}$ , was set to 4 in this study. We expect that better results could be obtained by adjusting this parameter appropriately, probably taking higher values for larger clusters or for compositions close to 50%. The amplitude of atomic displacement,  $h^{(p)}$ , is set to half the equilibrium distance in the  $\text{X}_2$  dimer for  $p = 0$ , half the equilibrium distance in the  $\text{Y}_2$  dimer for  $p = n$ , and is interpolated linearly between these two values for  $0 < p < n$ . In the present work, the exchange probabilities were taken as  $P_{\text{ex}} = 0.5$  and  $P_{\text{swap}} = 0.9$ , hence allowing a rather large probability of sampling among homotops of a same structure.

Low-energy structures for mixtures of xenon with either argon or krypton atoms have been first investigated for the sizes  $n = 13$  and  $n = 19$ , as there are quantitative global optimization data available for Ar–Xe clusters from the Jordan group.<sup>18</sup> It turns out that the energies of the structures given in Ref. 18 do not exactly match the values of the Lennard-Jones parameters used in this study, probably due to a possible round-off of these parameters. We have adjusted the values of Leitner *et al.*<sup>45</sup> to reproduce the clusters energies found by Munro and coworkers.<sup>18</sup> With respect to argon, the present data for  $\sigma$  and  $\varepsilon$  are thus  $\sigma_{\text{KrKr}} = 1.12403$ ,  $\sigma_{\text{XeXe}} = 1.206$ ,  $\sigma_{\text{KrXe}} = 1.16397$ ,  $\sigma_{\text{ArXe}} = 1.074$ ,  $\varepsilon_{\text{KrKr}} = 1.373534$ ,  $\varepsilon_{\text{XeXe}} = 1.852$ ,  $\varepsilon_{\text{KrXe}} = 1.59914$ , and  $\varepsilon_{\text{ArXe}} = 1.48$ . Global optimization of Ar–Xe and Kr–Xe clusters was performed using the parallel algorithm previously described, simultaneously for all compositions, for a maximum number of 10000 minimization steps per trajectory. Ten independent runs were carried out to estimate an average search length for each composition. All global minima reported by Munro *et al.* were always found within the number of MC steps allowed.

The results for  $\text{Ar}_n\text{Xe}_{13-n}$  and  $\text{Kr}_n\text{Xe}_{13-n}$  clusters are given in Table I. The average search length is generally higher for compositions close to 50%, for which the number of homotops is maximum for a given isomer, regardless of symmetry. The statistics presently obtained for Ar–Xe clusters show that the average search is between 10 and 1000 times faster than using conventional parallel basin-hopping.<sup>18</sup> Kr–Xe clusters roughly exhibit the same level of difficulty, but we do not see any strong ev-

idence for particularly severe cases:  $\text{Ar}_3\text{Xe}_{10}$  even seems to be one of the easiest.

Similarly, the results obtained for  $\text{Ar}_n\text{Xe}_{19-n}$  clusters show a significant improvement over fixed-composition basin-hopping.<sup>18</sup> They are given in Table II along with the corresponding data for  $\text{Kr}_n\text{Xe}_{19-n}$  clusters. This time, the algorithm is about 1–100 times faster depending on  $n$ , the average search length being still longer for equal compositions. For both the 13- and 19-atom clusters, all global minima are homotops of either the single or double icosahedron. This situation is particularly suited for our algorithm, especially the exchange moves.

Initially, the configurations at all compositions are random. The chances to locate the proper structure (without any consideration of the homotops) increase linearly with the number of trajectories. As soon as the right structure is found, the algorithm naturally optimizes atom types to find the most stable homotop, hence the global minimum. But it can also communicate the structure to the adjacent trajectories, until all compositions only need to sample among the permutational homotops.

When the interactions are not too dissimilar (as in Kr–Xe clusters), it is likely that the mixed clusters share the same isomer as the global minimum of the homogeneous cluster. The problem is then reduced to locating the most stable homotops. By setting  $P_{\text{swap}}$  to one and starting all trajectories from this minimum, the algorithm can be even more successful, and we estimated the average search length to be further reduced by a factor about 3 with respect to the values given in Table II. This version of the algorithm was applied to the 55-atom Ar–Xe clusters at all possible compositions, the results will be made available as supplementary material.<sup>46</sup> [see Table IV]

However, when the interactions differ significantly among atoms types, or when the energy landscape of the homogeneous cluster does not display a single steep funnel, it becomes much harder to make a guess about structure in these binary clusters.

### III. APPLICATION TO THE 38-ATOM CLUSTER

The  $\text{LJ}_{38}$  cluster is characterized by its archetypal two-funnel energy landscape.<sup>33</sup> The high free-energy barrier separating these two funnels and the higher entropy of the less stable minima of the icosahedral funnel make it particularly hard to locate the truncated octahedral lowest-energy minimum using unbiased global optimization algorithms. Hence it is not surprising that this peculiar structure was first found by construction.<sup>48,49</sup>

#### A. Composition-induced transitions

We have attempted to locate global minima for binary Ar–Xe and Kr–Xe clusters of size 38, using the parallel basin-hopping algorithm previously described. Because

TABLE I: Global optimization results for  $\text{Ar}_n\text{Xe}_{13-n}$  and  $\text{Kr}_n\text{Xe}_{13-n}$  clusters. The search length is the average over 10 independent runs of the number of Monte Carlo steps needed to find the global minimum. Energies are given in LJ units for argon.

$\text{Ar}_n\text{Xe}_{13-n}$ cluster	Global minimum energy	Average search length	$\text{Kr}_n\text{Xe}_{13-n}$ cluster	Global minimum energy	Average search length
$\text{Xe}_{13}$	-82.093	3.2	$\text{Xe}_{13}$	-82.093	3.0
$\text{ArXe}_{12}$	-78.698	7.9	$\text{KrXe}_{12}$	-81.014	9.6
$\text{Ar}_2\text{Xe}_{11}$	-76.274	9.6	$\text{Kr}_2\text{Xe}_{11}$	-79.263	4.3
$\text{Ar}_3\text{Xe}_{10}$	-74.015	5.8	$\text{Kr}_3\text{Xe}_{10}$	-77.550	5.7
$\text{Ar}_4\text{Xe}_9$	-71.597	8.6	$\text{Kr}_4\text{Xe}_9$	-75.869	26.1
$\text{Ar}_5\text{Xe}_8$	-69.017	14.0	$\text{Kr}_5\text{Xe}_8$	-74.186	25.8
$\text{Ar}_6\text{Xe}_7$	-66.584	37.2	$\text{Kr}_6\text{Xe}_7$	-72.498	26.4
$\text{Ar}_7\text{Xe}_6$	-63.791	19.4	$\text{Kr}_7\text{Xe}_6$	-70.844	45.2
$\text{Ar}_8\text{Xe}_5$	-60.733	13.9	$\text{Kr}_8\text{Xe}_5$	-69.141	18.3
$\text{Ar}_9\text{Xe}_4$	-57.851	22.7	$\text{Kr}_9\text{Xe}_4$	-67.473	4.7
$\text{Ar}_{10}\text{Xe}_3$	-54.594	12.0	$\text{Kr}_{10}\text{Xe}_3$	-65.802	11.5
$\text{Ar}_{11}\text{Xe}_2$	-51.122	7.5	$\text{Kr}_{11}\text{Xe}_2$	-64.128	4.1
$\text{Ar}_{12}\text{Xe}$	-47.698	4.1	$\text{Kr}_{12}\text{Xe}$	-62.490	2.4
$\text{Ar}_{13}$	-44.327	2.7	$\text{Kr}_{13}$	-60.884	2.3

TABLE II: Global optimization results for  $\text{Ar}_n\text{Xe}_{19-n}$  and  $\text{Kr}_n\text{Xe}_{19-n}$  clusters. The search length is the average over 10 independent runs of the number of Monte Carlo steps needed to find the global minimum. Energies are given in LJ units for argon.

$\text{Ar}_n\text{Xe}_{19-n}$ cluster	Global minimum energy	Average search length	$\text{Kr}_n\text{Xe}_{19-n}$ cluster	Global minimum energy	Average search length
$\text{Xe}_{19}$	-134.566	72.4	$\text{Xe}_{19}$	-134.566	70.7
$\text{ArXe}_{18}$	-131.819	64.3	$\text{KrXe}_{18}$	-133.651	94.0
$\text{Ar}_2\text{Xe}_{17}$	-129.116	80.3	$\text{Kr}_2\text{Xe}_{17}$	-132.701	109.8
$\text{Ar}_3\text{Xe}_{16}$	-126.547	85.2	$\text{Kr}_3\text{Xe}_{16}$	-130.088	84.3
$\text{Ar}_4\text{Xe}_{15}$	-123.764	238.2	$\text{Kr}_4\text{Xe}_{15}$	-129.067	167.2
$\text{Ar}_5\text{Xe}_{14}$	-120.786	196.6	$\text{Kr}_5\text{Xe}_{14}$	-127.284	175.4
$\text{Ar}_6\text{Xe}_{13}$	-118.278	221.2	$\text{Kr}_6\text{Xe}_{13}$	-125.498	265.9
$\text{Ar}_7\text{Xe}_{12}$	-115.682	391.8	$\text{Kr}_7\text{Xe}_{12}$	-123.709	334.6
$\text{Ar}_8\text{Xe}_{11}$	-113.075	387.9	$\text{Kr}_8\text{Xe}_{11}$	-121.951	319.5
$\text{Ar}_9\text{Xe}_{10}$	-110.242	264.2	$\text{Kr}_9\text{Xe}_{10}$	-120.115	287.1
$\text{Ar}_{10}\text{Xe}_9$	-107.531	295.8	$\text{Kr}_{10}\text{Xe}_9$	-118.304	243.6
$\text{Ar}_{11}\text{Xe}_8$	-104.576	193.8	$\text{Kr}_{11}\text{Xe}_8$	-116.521	187.4
$\text{Ar}_{12}\text{Xe}_7$	-101.811	235.5	$\text{Kr}_{12}\text{Xe}_7$	-114.736	214.3
$\text{Ar}_{13}\text{Xe}_6$	-98.110	158.5	$\text{Kr}_{13}\text{Xe}_6$	-112.947	201.3
$\text{Ar}_{14}\text{Xe}_5$	-94.396	247.3	$\text{Kr}_{14}\text{Xe}_5$	-111.189	188.8
$\text{Ar}_{15}\text{Xe}_4$	-90.438	121.3	$\text{Kr}_{15}\text{Xe}_4$	-108.863	176.5
$\text{Ar}_{16}\text{Xe}_3$	-86.328	131.2	$\text{Kr}_{16}\text{Xe}_3$	-106.609	115.1
$\text{Ar}_{17}\text{Xe}_2$	-81.907	97.3	$\text{Kr}_{17}\text{Xe}_2$	-104.332	10.2
$\text{Ar}_{18}\text{Xe}$	-77.298	86.8	$\text{Kr}_{18}\text{Xe}$	-102.036	98.1
$\text{Ar}_{19}$	-72.660	62.2	$\text{Kr}_{19}$	-99.801	69.8

of the huge number of homotops at this size, and most importantly because of the structural competition between icosahedra and truncated octahedra, we cannot be fully confident that the global optimization was successful. Therefore, the energies reported in Table III for

Ar–Xe clusters should be taken with caution, as they could probably be bettered. The same data for 38-atom Kr–Xe clusters is also available as supplementary material.<sup>46</sup> [see Table V]

Specifically to this cluster size, all minima found dur-

TABLE III: Global optimization results for  $\text{Ar}_n\text{Xe}_{38-n}$ . The energies are given in LJ units for argon, and the symmetry and mixing ratios defined by Eq. (1) are reported.

$n$	Mixing ratio	Energy	Point group	$n$	Mixing ratio	Energy	Point group
0	0	-173.928	$O_h$	20	0.58	-268.683	$C_1$
1	0.03	-179.232	$C_s$	21	0.59	-272.465	$C_1$
2	0.06	-186.333	$C_s$	22	0.56	-276.924	$C_s$
3	0.15	-191.890	$C_1$	23	0.61	-280.169	$C_s$
4	0.19	-197.767	$C_1$	24	0.60	-283.955	$C_{2v}$
5	0.22	-203.421	$C_s$	25	0.60	-287.679	$C_s$
6	0.25	-208.709	$C_s$	26	0.59	-290.973	$C_1$
7	0.28	-213.815	$C_1$	27	0.58	-294.157	$C_s$
8	0.32	-218.631	$C_s$	28	0.58	-297.320	$C_{2v}$
9	0.34	-223.491	$C_1$	29	0.56	-300.202	$C_{2v}$
10	0.36	-228.209	$C_1$	30	0.50	-303.484	$C_1$
11	0.39	-232.771	$C_1$	31	0.51	-305.987	$C_1$
12	0.40	-237.337	$C_1$	32	0.46	-308.404	$C_1$
13	0.43	-241.887	$C_s$	33	0.43	-310.521	$C_1$
14	0.44	-246.117	$C_1$	34	0.38	-311.708	$C_1$
15	0.45	-249.677	$C_s$	35	0.31	-313.772	$C_1$
16	0.46	-253.593	$C_s$	36	0.25	-315.988	$C_1$
17	0.46	-257.184	$C_s$	37	0.14	-318.860	$C_1$
18	0.46	-261.079	$C_s$	38	0	-322.115	$O_h$
19	0.56	-264.927	$C_1$				

ing the optimization process were categorized as either icosahedral or cubic-like, depending on the energy of the corresponding homogeneous isomer found by quenching. In cases where the cubic isomer was not found among the isomers, we performed additional optimizations starting from this structure, setting  $P_{\text{swap}}$  to one. This mainly occurred for Ar–Xe clusters. Eventually, two series of minima were obtained for each of the icosahedral and octahedral funnels. We did not find any decahedral isomer that could compete with these structural types, even though some evidence for stabilizing decahedra by doping was reported in Ref. 50.

We have represented in Fig. 1 the relative energy differences  $\Delta E = E_{\text{fcc}} - E_{\text{ico}}$  between the most stable icosahedral isomers and the most stable cubic isomers, as they were obtained from our optimization scheme, for both the Ar–Xe and Kr–Xe mixtures. Besides some strong variations sometimes seen from one composition to the next, and which can be attributed to usual finite-size effects, general trends can be clearly observed.

First,  $\text{Kr}_{38-n}\text{Xe}_n$  clusters are always most stable in the cubic shape. Actually, changing the composition most often further stabilizes truncated octahedra, and only rarely enhances the stability of icosahedra, which occurs for  $n > 29$  and  $n = 21$ . Conversely  $\text{Ar}_{38-n}\text{Xe}_n$  clusters are preferentially found icosahedral, exceptions being  $n > 35$  and  $n = 0$ . This is an example of a composition-induced structural transition between the two funnels of the energy landscape.

From a computational point of view, it should be noted

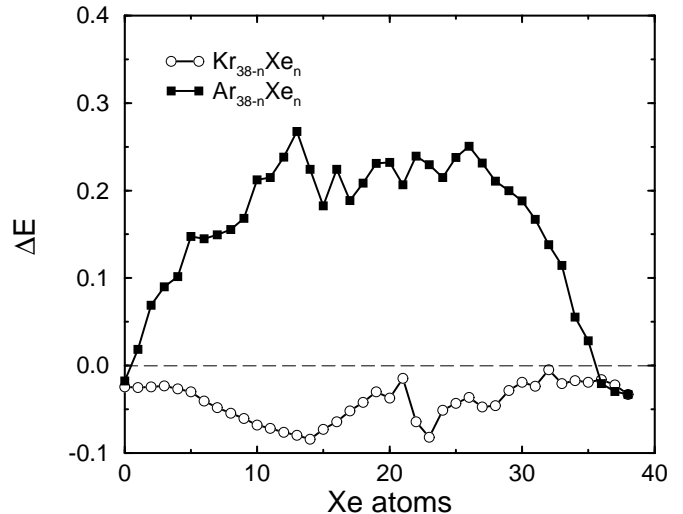


FIG. 1: Energy difference  $\Delta E = E_{\text{fcc}} - E_{\text{ico}}$  between the most stable octahedral and icosahedral isomers of  $\text{Kr}_{38-n}\text{Xe}_n$  (empty circles) and  $\text{Ar}_{38-n}\text{Xe}_n$  (full squares).  $\Delta E$  is given in reduced Lennard-Jones unit of Argon (approximately 120 K).

that the optimization algorithm was able to locate the truncated octahedral minima for Kr–Xe clusters by itself, starting from disordered minima, and that the extra runs starting from this structure only produced slightly more stable homotops. This is another illustration of the efficiency of the present parallel optimization method.

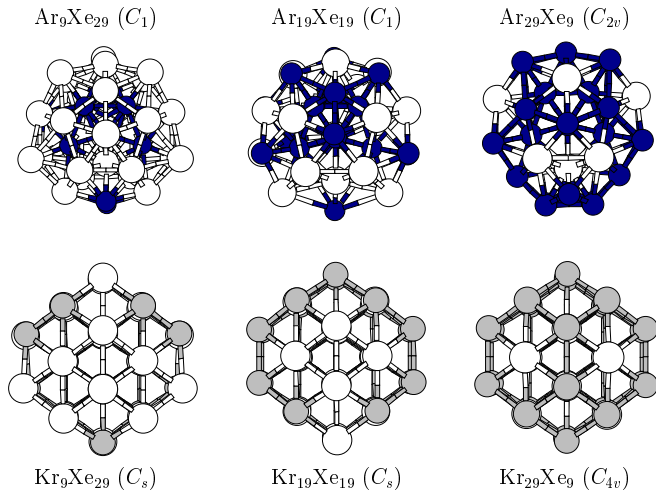


FIG. 2: Putative global minima found for several  $\text{Ar}_{38-n}\text{Xe}_n$  and  $\text{Kr}_{38-n}\text{Xe}_n$  clusters. Argon, krypton, and xenon atoms are represented as white, black, and gray balls, respectively. All structures have no particular symmetry.

The general degree of disorder is higher in icosahedral structures than in the cubic-like isomer. Hence it is more difficult to put up the latter geometry with very unlike interactions, as in Ar–Xe clusters. Cubic homotops of argon with xenon are rather distorted, but the strain is much lower with krypton instead of argon. Examples of global minima obtained at compositions  $n = 9, 19,$  and  $29$  are represented in Fig. 2. In Kr–Xe compounds, a progressive core-surface phase separation is seen with Kr atoms outside, in agreement with energetic arguments. In general, no complete phase separation is found in the Ar–Xe clusters, even though Ar atoms seem to fit best at the centre of the cluster. In both cases, surface energies thus play an important role. Mixing in these clusters can be estimated using radial distribution functions.<sup>47</sup> Here we use the same index as Jellinek and Krissinel,<sup>4</sup> namely the overall mixing ratio  $\gamma$  defined as<sup>4</sup>

$$\gamma(X_p Y_{n-p}) = \frac{E_{X_p Y_{n-p}} - E_{X_p}(X_p X_{n-p}) - E_{Y_{n-p}}(Y_p Y_{n-p})}{E_{X_p Y_{n-p}}}, \quad (1)$$

where  $E_{X_p Y_{n-p}}$  is the binding energy of cluster  $X_p Y_{n-p}$ ,  $E_{X_p}(X_p X_{n-p})$  the binding energy of subcluster  $X_p$  in the homogeneous cluster  $X_p X_{n-p}$  at the same atomic configuration as  $X_p Y_{n-p}$ , and a similar definition for the last term of Eq. (1). As seen from Table III, the mixing ratio increases notably in Ar–Xe clusters, up to more than 60% for some compositions. Kr–Xe clusters, despite exhibiting some core-surface segregation, show similar variations of the mixing ratio with composition, with only slightly smaller values of  $\gamma$ . Therefore the mixing ratio, as defined in Eq. (1), is a rather ambiguous parameter for quantifying the extent of mixing in this small cluster.

The optimal structure of an homogeneous cluster described with a pairwise potential results from a compe-

titition between maximizing the number of nearest neighbors and minimizing the strain energy, or penalty induced by distorting these bonds.<sup>49</sup> Binary Lennard-Jones systems exhibit several extra complications due to the various ways of rearranging atom types in a given structure. In these systems, the strain varies notably among the homotops, especially in clusters made of very unlike atoms. However, our results indicate that the same general rules hold for homogeneous and heterogeneous systems. In  $\text{Ar}_{19}\text{Xe}_{19}$ , the strain is rather high, but the number of contacts is also high. In  $\text{Kr}_{19}\text{Xe}_{19}$ , both the strain and the number of nearest neighbors are much smaller.

To investigate the role of heterogeneity on the strain, we have computed the various contributions to the reduced strain energies in  $\text{Ar}_{38-n}\text{Xe}_n$  clusters. The strain energies are defined for Ar–Ar, Xe–Xe, and Ar–Xe interactions as follows:<sup>49</sup>

$$\begin{aligned} E_{\text{Ar-Ar}}^{\text{strain}} &= V_{\text{Ar-Ar}}^{\text{LJ}} + N_{\text{Ar-Ar}}^{\text{nn}} \varepsilon_{\text{Ar-Ar}}, \\ E_{\text{Ar-Xe}}^{\text{strain}} &= V_{\text{Ar-Xe}}^{\text{LJ}} + N_{\text{Ar-Xe}}^{\text{nn}} \varepsilon_{\text{ArXe}}, \\ E_{\text{Xe-Xe}}^{\text{strain}} &= V_{\text{Xe-Xe}}^{\text{LJ}} + N_{\text{Xe-Xe}}^{\text{nn}} \varepsilon_{\text{Xe-Xe}}. \end{aligned}$$

In these equations,  $V_{X-Y}^{\text{LJ}}$  is the total binding energy between atoms  $X$  and  $Y$ ,  $N_{X-Y}^{\text{nn}}$  is the number of X–Y nearest neighbours, and  $\varepsilon_{X-Y}$  is the Lennard-Jones well depth corresponding to the interaction between  $X$  and  $Y$  atoms. Reduced strain energies are then defined as  $e^{\text{strain}} = E^{\text{strain}}/N^{\text{nn}}\varepsilon$ , in order to account for the different magnitudes of the interactions among atom types. The strain energies in  $\text{Ar}_{38-n}\text{Xe}_n$  clusters are represented versus composition in Fig. 3. They give us some insight about the possible ways of reducing strain.

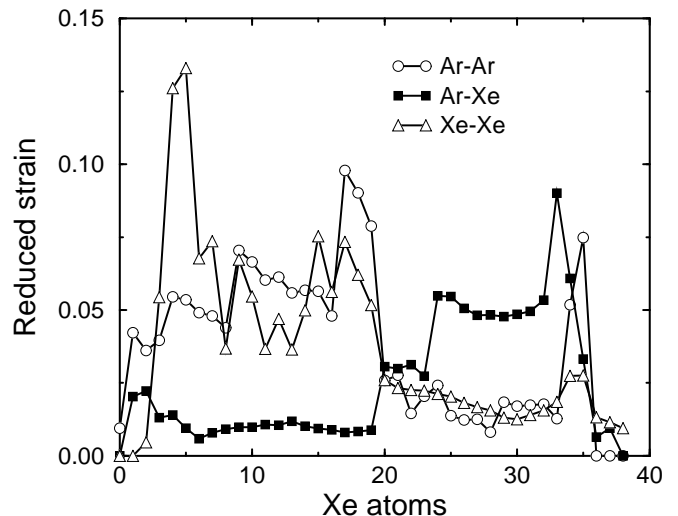


FIG. 3: Reduced strain energies for alike and unlike interactions in  $\text{Ar}_{38-n}\text{Xe}_n$  clusters, versus composition  $n$ .

The pattern exhibited by the reduced strain versus composition exhibits different behaviors for clusters having mostly argon or xenon atoms. For  $n < 20$ , most

strain is carried by interactions between alike atoms. This case is illustrated by  $\text{Ar}_9\text{Xe}_{29}$  in Fig. 2, where a kind of core/surface phase separation occurs. Here surface energies are crucial. Above this size, the reverse situation takes place, and interactions between the unlike atoms are significantly more strained. The case of  $\text{Ar}_{29}\text{Xe}_9$  depicted in Fig. 2 is particularly informative: Xe atoms are located scarcely among the icosahedral cluster, and relieve the structure from too much strain at the expense of only few Xe–Xe interactions. In this case, cluster structure is driven by the number of unlike interactions.

It is also worth noting that a few compositions are especially weakly strained; this occurs when the global minimum is octahedral, but also in the range  $19 < n < 24$ . For these latter clusters, the core/surface segregation and the number of unlike interactions are both optimal.

### B. Temperature-induced transitions

The extremely large number of isomers (including homotops) in the energy landscape of binary Lennard-Jones clusters, added to the expected presence of significant energy barriers between icosahedral and cubic isomers,<sup>33</sup> prevent finite-temperature simulations from being conducted in a reliably ergodic way with the presently available tools. For example, the particle exchange moves used to accelerate convergence of sampling among homotops will likely have very low acceptance probabilities in MC simulations at low temperatures, especially for Ar–Xe clusters. Therefore, even with powerful methods such as parallel tempering or multicanonical Monte Carlo, reaching convergence in 38-atom LJ clusters does not seem currently feasible to us.

As an alternative, we have chosen to investigate solid-solid transitions by means of the superposition approach.<sup>51,52</sup> For a given cluster, databases of minima in each of the icosahedral (ICO) and truncated octahedral (FCC) funnels were constructed using the optimization algorithm. For each composition and each of the two funnels, no more than 2000 distinct minima were considered. The classical partition function of the  $\text{Y}_{38-p}\text{Xe}_p$  cluster (Y=Ar or Kr) restricted to funnel A=FCC or ICO is approximated by a harmonic superposition over all minima of the databases, which belong to this funnel:<sup>52</sup>

$$Q_A(\beta) = \sum_{i \in A} n_i \frac{\exp(-\beta E_i)}{(\beta h \bar{\nu}_i)^{3n-6}}, \quad (2)$$

where  $\beta = 1/k_B T$  is the inverse temperature,  $\bar{\nu}_i$  the geometric mean vibrational frequency,  $n_i = 2p!(n-p)!/h_i$  with  $h_i$  the order of the point group of minimum  $i$  and  $n = 38$ . We do not consider quantum effects here, although they may be important at low temperatures,<sup>53</sup> since delocalization or zero-point effects are not expected to be significant for rare gases as heavy as krypton or xenon.

Within the harmonic superposition approximation, a solid-solid transition occurs when  $Q_{\text{FCC}} = Q_{\text{ICO}}$ .<sup>54</sup> This

latter equation is solved numerically in  $\beta$  or  $T$ , its solution is denoted  $T_{\text{ss}}$ . In cases where icosahedra are energetically more stable than octahedra, a solid-solid transition can occur if some cubic structures are entropically favored, which requires lower vibrational frequencies and/or lower symmetries. We did not find such situations in our samples of Ar–Xe clusters, therefore we restrict to Kr–Xe clusters in the following.

Similar to transitions between funnels, transitions between homotops will happen if their partition functions are equal. The huge number of homotops gives rise to as many values for the corresponding temperatures, and we define the homotop transition temperature  $T_h$  such that

$$T_h = \min_j \{T_h^{(j)} \mid T_h^{(j)} > 0\}, \quad (3)$$

where  $T_h^{(j)}$  is the transition temperature between the global minimum (homotop 0) and its homotop  $j$ . Equating the harmonic partition functions for these two isomers leads to the expression of  $T_h^{(j)}$ :<sup>54</sup>

$$k_B T_h^{(j)} = \frac{E_j - E_0}{(3n-6) \ln \bar{\nu}_0 / \bar{\nu}_j + \ln n_j / n_0}. \quad (4)$$

Since all homotops are characterized by different vibrational and symmetry properties, the transition temperatures  $T_h^{(j)}$  are not ordered exactly as the energy differences  $E_j - E_0$ . This reflects that solid-solid transitions involve crossover in free energy rather than binding energy. The above equation also shows that  $T_h^{(j)}$  can take negative values if homotop  $j$  has a higher symmetry and/or a higher vibrational frequency than the ground state. In this case the global minimum is always the free energy minimum, and no solid-solid transition occurs, hence the form of Eq. (3).

Finally, a third temperature has a strong consequence on cluster structure, namely the melting temperature. Its estimation from either simulations or superpositions approximations is already quite difficult for the homogeneous LJ<sub>38</sub> cluster,<sup>33,34</sup> and we did not attempt to compute it for binary clusters. However, the previous study by Frantz<sup>15</sup> has shown that the melting point in mixed, 13-atom Ar–Kr clusters varies quite regularly (approximately quadratically) with composition. We have used an even simpler rule here, by assuming that the melting point of  $\text{Kr}_{38-n}\text{Xe}_n$ ,  $T_{\text{melt}}(n)$ , is related *linearly* to the melting points  $T_{\text{melt}}(0)$  and  $T_{\text{melt}}(38)$  of  $\text{Kr}_{38}$  and  $\text{Xe}_{38}$ , respectively. From the results obtained by Doye and Wales<sup>33</sup> and the Monte Carlo data of Ref. 34 for the LJ<sub>38</sub> cluster, we get  $T_{\text{melt}}(0) \simeq 0.234$  and  $T_{\text{melt}}(38) \simeq 0.315$  in reduced LJ units of argon. This linear approximation obviously neglects finite-size effects, but will provide a rough estimation.

The transition temperatures are represented in Fig. 4 for all compositions in  $\text{Kr}_{38-n}\text{Xe}_n$  clusters. We notice first that the structural transition temperature  $T_{\text{ss}}$  varies quite regularly with composition in both the ranges  $n < 19$  and  $n > 21$ , and that it shows strong size effects

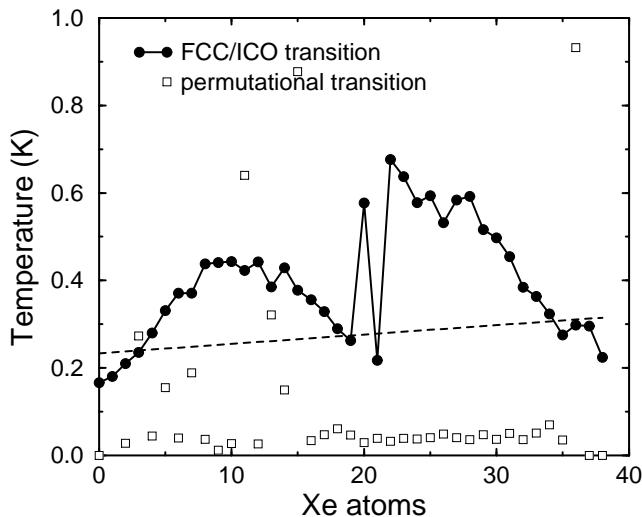


FIG. 4: Solid-solid transition temperature (full circles) between the octahedral and icosahedral funnels, estimated from a harmonic superposition approximation, versus composition in  $\text{Kr}_n\text{Xe}_{38-n}$  clusters. Also shown is the lowest transition temperature for a permutation between octahedral homotops.

between these limits. Several situations are predicted to occur depending on the relative values of  $T_{ss}$ ,  $T_h$  and  $T_{\text{melt}}$ .

In most cases,  $T_{\text{melt}} < T_{ss}$ . That melting takes place at temperatures lower than the cubic/icosahedral transition simply nullifies the transition between structural types. However, this extra stability of the octahedral funnel may have a consequence on the melting point itself, which is likely to increase. Still, this situation implies that simulations will more easily reach convergence.

However, there are notable exceptions for this behavior, at  $n < 4$ ,  $n = 21$  and  $n > 34$ . In these clusters, heterogeneity is not sufficient for the thermodynamical behavior of the cluster to deviate too much from those of the homogeneous system.

The transition between homotops usually occurs prior to melting. Thermal equilibrium within the cubic funnels thus involve several homotops (and “restricted” solid-solid transitions), and the corresponding thermodynamical state could be probably simulated using specifically designed exchange moves between outer particles within a Monte Carlo scheme.

A few clusters melt before exhibiting any transition between homotops. This occurs for instance at  $n = 11$ , 13 or 15. For these sizes the structural transition also occurs at temperatures higher than the estimated melting point. These cases should pose less problems to conventional simulations than the homogeneous cluster.

### C. Glassy behavior

The previous results have shown that finite-size Ar–Xe compounds show a preferential icosahedral order, even for very low doping rates, over octahedral order. The reverse seems to hold for Kr–Xe clusters at the same size. Since icosahedral order is known to be present in liquids and, more generally, in disordered structural glasses, it seems natural to correlate the behavior observed in these clusters to the dynamics of the corresponding bulk materials.<sup>22</sup>

We have simulated the cooling of 108-atom binary rare-gas liquids, using a simple Metropolis Monte Carlo scheme under constant volume and temperature. Initially the atoms are placed randomly into a cubic box of side  $L$ , and periodic boundaries are treated in the minimum image convention. The LJ interactions were not truncated, and the simulations consisted of 100 stages of  $10^5$  MC cycles each, linearly spaced in temperature.

Three compositions have been selected, following our knowledge of the cluster structure. For each composition, different length sizes  $L$  and different temperature ranges  $[T_{\text{min}}, T_{\text{max}}]$  were chosen in order to cover both sides of the melting point. In the first mixture, 24 xenon atoms and 84 argon atoms are simulated with  $L = 4.8815$  LJ units of argon, with  $0.1 \leq T \leq 1$ . In the second mixture, 24 xenon atoms are added to 84 krypton atoms at  $L = 5.487$  and  $0.15 \leq T \leq 1.5$ . The third mixture consists of 9 argon atoms and 99 xenon atoms at  $L = 5.887$  and  $0.2 \leq T \leq 2$ . Even though we did not attempt to locate the most stable crystalline forms for these mixtures, our searches close to the face-centred cubic morphology showed that the most stable configurations for these mixtures always had some cubic order. It is likely that the actual ground states for such systems are indeed crystalline.<sup>55</sup>

The average root mean square fluctuation of the bond distances, also known as the Lindemann index  $\delta$ , universally characterizes the thermodynamical state of the condensed system as either solid or liquid, depending on its value being lower or higher than about 0.15. To quantify the extent of crystalline order, we have used the bond order parameter  $Q_4$  introduced by Steinhardt and coworkers.<sup>56</sup> The two parameters  $\delta$  and  $Q_4$  allow us to follow in Monte Carlo time the cooling processes for all materials in a simultaneous way, independently of thermodynamical characteristics such as the melting temperature.

The correlation between  $\delta$  and  $Q_4$  for ten cooling simulations of each of the three bulk binary compounds is represented in Fig. 5. In all cases, the Lindemann parameter covers the whole range  $0.01 < \delta < 0.18$ , indicating that the melting point was indeed crossed. However, the three compounds display very contrasted cooling behaviors.

In the  $(\text{Ar}_{84}\text{Xe}_{24})$  system,  $\delta$  regularly decreases but  $Q_4$  always remain below 0.05. Therefore crystallization never takes place, and the final state obtained by quench-



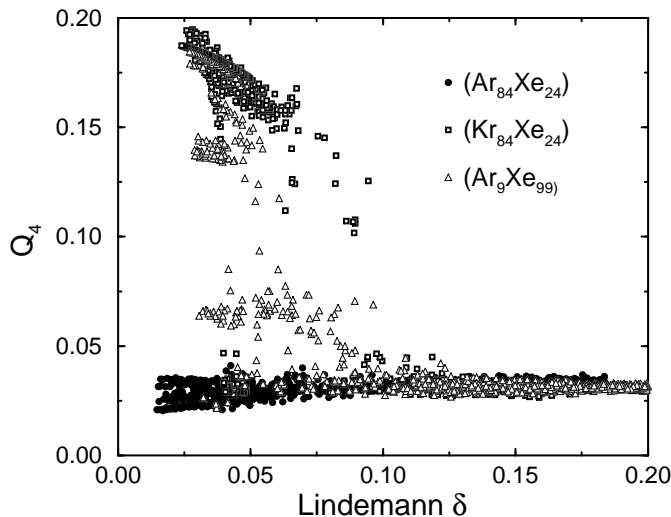


FIG. 5: Correlation between the Lindemann parameter  $\delta$  and the order parameter  $Q_4$  along cooling simulations of Ar–Xe and Kr–Xe bulk mixtures.

ing is significantly higher in energy than some crystalline forms; this is typical of glass formation.

In ( $\text{Kr}_{84}\text{Xe}_{24}$ ), all simulations show some rather sharp transition from a (high  $\delta$ , low  $Q_4$ ) state to a (low  $\delta$ , high  $Q_4$ ) state as  $\delta$  crosses about 0.1. The temperatures where crystallisation occurs may vary somewhat among the cooling runs, in the same way as they are expected to depend on the cooling rate.

Lastly, the case of ( $\text{Ar}_9\text{Xe}_{99}$ ) is intermediate: while most simulations end up in a nearly fully crystalline phase ( $Q_4 \sim 0.15$ ), a few of them show a limited degree of cubic ordering in the solid phase,  $Q_4$  having values close to 0.07.

These results very closely reflect our previous data on binary, 38-atom clusters of the same materials. In terms of composition, the first mixture corresponds to  $\text{Ar}_{30}\text{Xe}_8$ , which clearly favors icosahedral shapes over truncated octahedra. The second mixture reminds of  $\text{Kr}_{30}\text{Xe}_8$ , for which the cubic structure is even more stable than in the homogeneous cluster. The third mixture should be compared to  $\text{Ar}_3\text{Xe}_{35}$ , which favors icosahedra only moderately.

This correlation found here between cluster structure and the glassforming ability of the bulk material confirms previous analyses on the icosahedral local order in liquids and glasses,<sup>22,31</sup> as well as the recent conclusions obtained by Doye *et al.*<sup>32</sup> that clusters of good glassformers indeed show a polytetrahedral order.

#### IV. CONCLUSION

As far as structural and dynamical properties are concerned, binary compounds show a significantly richer complexity with respect to homogeneous clusters. The

work reported in the present paper was intended to achieve several goals. First, a parallel global optimization algorithm was designed to locate the most stable structures of mixed rare-gas clusters. Based on the basin-hopping or Monte Carlo+minimization algorithm,<sup>37,38</sup> this algorithm includes exchange moves between particles at fixed composition as well as exchange moves between configurations at different compositions. Tests on simple  $\text{Ar}_n\text{Xe}_{13-n}$  and  $\text{Ar}_n\text{Xe}_{19-n}$  clusters show that the method is quite efficient, in addition to being easy to implement.

Putative global minima for  $\text{Ar}_{38-n}\text{Xe}_n$  and  $\text{Kr}_{38-n}\text{Xe}_n$  clusters have been investigated for all compositions. The structure of Ar–Xe compounds is mainly icosahedral, except at very low doping rates. Kr–Xe clusters not only remain as truncated octahedra, but mixing the two rare gases even favors these cubic structures over icosahedra. We see some significant trend toward core/surface phase separation in Ar–Xe clusters with  $n > 20$  and in all Kr–Xe clusters. Conversely,  $\text{Ar}_{38-n}\text{Xe}_n$  clusters with  $n < 20$  exhibit a higher degree of mixing. Analysing the strain in these stable structures confirms the presence of a structural transition near  $n = 20$  in these systems.

Within the harmonic superposition approximation, we have estimated the temperatures required by the 38-atom Kr–Xe clusters to undergo a structural transition toward the icosahedral funnel, or toward other octahedral homotops. For compositions with a doping rate higher than 3/38, the structural transition temperature was seen to occur at temperatures higher than the extrapolated melting point. This mainly reflects the special stability of the octahedral structures, and has the probable consequence that actual melting points increase somewhat. These predictions could probably be checked with numerical simulations. For most compositions, the transitions between different homotops of the truncated octahedron are seen to be potentially induced by relatively small temperatures. Therefore particle exchange moves will be necessary in order that simulations remain close to ergodic.

Finally, and following previous results by other researchers,<sup>22,31,32</sup> we have found some further evidence that criteria for glass formation in bulk materials may also lie in the parameters, which are responsible for stable cluster structures. Since the atomistic simulation of the dynamical vitrification process can generally be much harder than obtaining stable configurations of atomic clusters, we expect the approach followed in the present theoretical effort to be also useful in the community of glasses and supercooled liquids.

The method is obviously not limited to rare-gases, and its application to other compounds, especially metallic nanoalloys, is straightforward. From a methodological point of view, it could also be applied to materials with more than two components. Work on ternary systems is currently in progress.

### Acknowledgments

We wish to thank Dr. J. P. K. Doye and Prof. K. J. Jordan for very useful discussions. This research was

supported by the CNRS-TUBITAK grant number 15071.

- 
- <sup>1</sup> S. Chacko, M. Deshpande, and D. G. Kanhere, *Phys. Rev. B* **64**, 155409 (2001).
- <sup>2</sup> S. Bromley, G. Sankar, C. R. A. Catlow, T. Maschmeyer, B. F. G. Johnson, and J. M. Thomas, *Chem. Phys. Lett.* **340**, 524 (2001).
- <sup>3</sup> B. K. Rao, S. R. de Debiaggi, and P. Jena, *Phys. Rev. B* **64**, 024418 (2001).
- <sup>4</sup> J. Jellinek and E. B. Krissinel, *Chem. Phys. Lett.* **258**, 283 (1996); E. B. Krissinel and J. Jellinek, *ibid.* **272**, 301 (1997).
- <sup>5</sup> J. L. Rousset, A. M. Cadrot, F. J. Cadete Santos Aires, A. Renouprez, P. Mélinon, A. Perez, M. Pellarin, J. L. Vialle, and M. Broyer, *J. Chem. Phys.* **102**, 8574 (1995).
- <sup>6</sup> M. J. López, P. A. Marcos, and J. A. Alonso, *J. Chem. Phys.* **104**, 1056 (1996).
- <sup>7</sup> G. E. López and D. L. Freeman, *J. Chem. Phys.* **98**, 1428 (1993).
- <sup>8</sup> I. L. Garzon, X. P. Long, R. Kawai, and J. H. Weare, *Chem. Phys. Lett.* **158**, 525 (1989).
- <sup>9</sup> P. Ballone, W. Andreoni, R. Car, and M. Parrinello, *Europhys. Lett.* **8**, 73 (1989).
- <sup>10</sup> S. Darby, T. V. Mortimer-Jones, R. L. Johnston, and C. Roberts, *J. Chem. Phys.* **116**, 1536 (2002).
- <sup>11</sup> M. S. Bailey, N. T. Wilson, C. Roberts, and R. L. Johnston, *Euro. Phys. J. D* **25**, 41 (2003).
- <sup>12</sup> M. C. Vicéns and G. E. López, *Phys. Rev. A* **62**, 033203 (2000).
- <sup>13</sup> F. Baletto, C. Mottet, and R. Ferrando, *Phys. Rev. Lett.* **90**, 135504 (2003).
- <sup>14</sup> J. P. K. Doye, M. A. Miller, and D. J. Wales, *J. Chem. Phys.* **111**, 8417 (1999).
- <sup>15</sup> D. D. Frantz, *J. Chem. Phys.* **105**, 10030 (1996).
- <sup>16</sup> D. D. Frantz, *J. Chem. Phys.* **107**, 1992 (1997).
- <sup>17</sup> G. S. Fanourgakis, P. Parneix, and Ph. Bréchnignac, *Euro. Phys. J. D* **24**, 207 (2003).
- <sup>18</sup> L. J. Munro, A. Tharrington, and K. J. Jordan, *Comp. Phys. Comm.* **145**, 1 (2002).
- <sup>19</sup> P. Parneix, Ph. Bréchnignac, and F. Calvo, *Chem. Phys. Lett.* **381**, 471 (2003).
- <sup>20</sup> F. Calvo, J. P. K. Doye, and D. J. Wales, *J. Chem. Phys.* **116**, 2642 (2002).
- <sup>21</sup> A. S. Clarke, R. Kapral, B. Moore, G. Patey, and X.-G. Wu, *Phys. Rev. Lett.* **70**, 3283 (1993); A. S. Clarke, R. Kapral, and G. N. Patey, *J. Chem. Phys.* **101**, 2432 (1994).
- <sup>22</sup> H. Jónsson and H. C. Andersen, *Phys. Rev. Lett.* **60**, 2295 (1988).
- <sup>23</sup> W. Kob and H. C. Andersen, *Phys. Rev. E* **51**, 4626 (1995).
- <sup>24</sup> B. Coluzzi, G. Parisi, and P. Verocchio, *J. Chem. Phys.* **112**, 2933 (2000).
- <sup>25</sup> M. Utz, P. G. Debenetti, F. H. Stillinger, *Phys. Rev. Lett.* **84**, 1471 (2000).
- <sup>26</sup> K. K. Bhattacharya, K. Broderix, R. Kree, and A. Zippehus, *Europhys. Lett.* **47**, 449 (1999).
- <sup>27</sup> R. Yamamoto and W. Kob, *Phys. Rev. E* **61**, 5473 (2000).
- <sup>28</sup> H.-J. Lee, T. Cagin, W. L. Johnson, and W. A. Goddard, *J. Chem. Phys.* **119**, 9858 (2003).
- <sup>29</sup> F. C. Frank, *Proc. R. Soc. London, Ser. A* **215**, 43 (1952).
- <sup>30</sup> T. Schenk, D. Holland-Moritz, V. Simonet, R. Bellissent, and D. M. Herlach, *Phys. Rev. Lett.* **89**, 075507 (2002).
- <sup>31</sup> S. Mossa and G. Tarjus, *J. Chem. Phys.* **119**, 8069 (2003).
- <sup>32</sup> J. P. K. Doye, D. J. Wales, F. H. M. Zetterling, and M. Dzugutov, *J. Chem. Phys.* **118**, 2792 (2003).
- <sup>33</sup> J. P. K. Doye, M. A. Miller, and D. J. Wales, *J. Chem. Phys.* **110**, 6896 (1999).
- <sup>34</sup> J. P. Neirotti, F. Calvo, D. L. Freeman, and J. D. Doll, *J. Chem. Phys.* **112**, 10340 (2000).
- <sup>35</sup> D. J. Wales and H. A. Scheraga, *Science* **285**, 1368 (1999).
- <sup>36</sup> B. Hartke, *Chem. Phys. Lett.* **258**, 144 (1996).
- <sup>37</sup> Z. Li and H. A. Scheraga, *Proc. Natl. Acad. Sci. USA* **84**, 6611 (1987).
- <sup>38</sup> D. J. Wales and J. P. K. Doye, *J. Phys. Chem. A* **101**, 5111 (1997).
- <sup>39</sup> D. J. Wales, J. P. K. Doye, A. Dullweber, M. P. Hodges, F. Y. Naumkin, F. Calvo, J. Hernández-Rojas and T. F. Middleton, URL <http://www-wales.ch.cam.ac.uk/CCD.html>.
- <sup>40</sup> G. J. Geyer, in *Computing Science and Statistics: Proceedings of the 23rd Symposium on the Interface*, ed. by E. K. Keramidas (Interface Foundation, Fairfax Station, 1991), p. 156.
- <sup>41</sup> D. Gazzillo and G. Pastore, *Chem. Phys. Lett.* **159**, 388 (1989).
- <sup>42</sup> H. Karaaslan and E. Yurtsever, *Chem. Phys. Lett.* **187**, 8 (1991).
- <sup>43</sup> T. S. Grigera and G. Parisi, *Phys. Rev. E* **63**, 045102(R) (2001).
- <sup>44</sup> R. H. Leary and J. P. K. Doye, *Phys. Rev. E* **60**, R6320 (1999).
- <sup>45</sup> D. M. Leitner, J. D. Doll, and R. M. Whitnell, *J. Chem. Phys.* **94**, 6644 (1991).
- <sup>46</sup> F. Calvo and E. Yurtsever, physics/04XXXXX.
- <sup>47</sup> H. Karaaslan and E. Yurtsever, *Ber. Bunsenges. Phys. Chem.* **98**, 47 (1994).
- <sup>48</sup> J. Pillardy and L. Piela, *J. Phys. Chem.* **99**, 11805 (1995).
- <sup>49</sup> J. P. K. Doye, D. J. Wales, and R. S. Berry, *J. Chem. Phys.* **103**, 4234 (1995).
- <sup>50</sup> F. Calvo, F. Spiegelman, and M.-C. Heitz, *J. Chem. Phys.* **118**, 8739 (2003).
- <sup>51</sup> F. H. Stillinger and T. A. Weber, *Phys. Rev. A* **25**, 978 (1982).
- <sup>52</sup> D. J. Wales, *Mol. Phys.* **78**, 151 (1993).
- <sup>53</sup> F. Calvo, J. P. K. Doye, and D. J. Wales, *J. Chem. Phys.* **114**, 7312 (2001).
- <sup>54</sup> J. P. K. Doye and F. Calvo, *Phys. Rev. Lett.* **86**, 3570 (2001).
- <sup>55</sup> T. F. Middleton, J. Hernández-Rojas, P. N. Mortenson, and D. J. Wales, *Phys. Rev. B* **64**, 184201 (2001); J. R. Fernández and P. Harrowell, *Phys. Rev. E* **67**, 011403 (2003).
- <sup>56</sup> P. J. Steinhardt, D. R. Nelson, and M. Ronchetti, *Phys. Rev. B* **28**, 784 (1983).

TABLE IV: Global optimization results for  $\text{Ar}_{55-n}\text{Xe}_n$ . The energies are given in LJ units for argon, and the symmetry and mixing ratios defined by Eq. (1) are reported.

$n$	Mixing ratio	Energy	Point group	$n$	Mixing ratio	Energy	Point group
0	0	-279.248	$I_h$	28	0.53	-417.720	$C_1$
1	0.05	-284.276	$C_{2v}$	29	0.53	-420.844	$C_1$
2	0.10	-289.313	$D_1$	30	0.51	-423.667	$C_1$
3	0.15	-294.360	$C_s$	31	0.49	-427.764	$C_1$
4	0.21	-299.391	$C_1$	32	0.48	-431.062	$C_1$
5	0.25	-304.619	$C_s$	33	0.44	-433.643	$C_1$
6	0.39	-310.143	$C_1$	34	0.43	-437.429	$C_2$
7	0.43	-316.489	$C_1$	35	0.43	-441.317	$C_1$
8	0.43	-322.175	$C_1$	36	0.41	-445.584	$C_1$
9	0.46	-327.615	$C_1$	37	0.41	-449.549	$C_1$
10	0.48	-333.240	$C_1$	38	0.35	-453.515	$C_1$
11	0.52	-338.719	$C_s$	39	0.35	-458.203	$C_s$
12	0.53	-343.833	$C_1$	40	0.34	-462.564	$C_{2v}$
13	0.55	-349.126	$C_1$	41	0.30	-466.709	$C_{2v}$
14	0.56	-354.452	$C_1$	42	0.28	-472.191	$I_h$
15	0.57	-359.498	$C_1$	43	0.26	-475.967	$C_{5v}$
16	0.58	-365.268	$C_1$	44	0.24	-479.739	$D_{5d}$
17	0.59	-370.295	$C_1$	45	0.22	-483.495	$C_{3v}$
18	0.59	-375.713	$C_1$	46	0.20	-487.219	$C_{2v}$
19	0.59	-380.585	$C_1$	47	0.18	-490.910	$C_s$
20	0.60	-384.610	$C_1$	48	0.16	-494.585	$C_2$
21	0.60	-389.950	$C_1$	49	0.14	-498.231	$C_s$
22	0.59	-395.065	$C_1$	50	0.12	-501.860	$C_{2v}$
23	0.59	-399.086	$C_1$	51	0.10	-505.467	$C_{3v}$
24	0.60	-403.205	$C_1$	52	0.08	-509.052	$D_{5d}$
25	0.58	-406.983	$C_1$	53	0.06	-512.616	$C_{5v}$
26	0.56	-410.562	$C_1$	54	0.04	-516.170	$I_h$
27	0.56	-414.195	$C_1$	55	0	-517.168	$I_h$

TABLE V: Global optimization results for  $\text{Kr}_n\text{Xe}_{38-n}$ . The energies are given in LJ units for argon, and the symmetry and mixing ratios defined by Eq. (1) are reported.

$n$	Mixing ratio	Energy	Point group	$n$	Mixing ratio	Energy	Point group
0	0	-238.897	$O_h$	20	0.45	-286.209	$C_s$
1	0.09	-241.200	$C_s$	21	0.44	-288.240	$C_s$
2	0.18	-243.604	$C_{2v}$	22	0.42	-290.323	$C_{2v}$
3	0.25	-245.962	$C_s$	23	0.42	-292.310	$C_s$
4	0.27	-248.453	$C_s$	24	0.41	-294.347	$O_h$
5	0.33	-250.927	$C_s$	25	0.37	-296.352	$C_{3v}$
6	0.35	-253.489	$C_{2v}$	26	0.35	-298.371	$C_{2v}$
7	0.39	-256.005	$C_s$	27	0.33	-300.382	$C_s$
8	0.41	-258.570	$D_{4h}$	28	0.32	-302.414	$C_{4v}$
9	0.43	-261.156	$C_s$	29	0.29	-304.411	$C_{4v}$
10	0.45	-263.740	$C_{2v}$	30	0.25	-306.457	$C_s$
11	0.47	-266.294	$C_s$	31	0.22	-308.390	$C_s$
12	0.48	-268.867	$C_s$	32	0.20	-310.370	$C_s$
13	0.49	-271.420	$C_s$	33	0.16	-312.315	$C_s$
14	0.50	-273.996	$C_{2v}$	34	0.13	-314.287	$C_{3v}$
15	0.50	-275.996	$C_s$	35	0.10	-316.230	$C_s$
16	0.50	-278.046	$D_{4h}$	36	0.07	-318.200	$D_{4h}$
17	0.48	-280.082	$C_s$	37	0.04	-320.133	$C_{4v}$
18	0.47	-282.129	$C_{2v}$	38	0	-322.115	$O_h$
19	0.46	-284.164	$C_s$				